Mitochondrial Bovine ADP/ATP Carrier in Detergent Is Predominantly Monomeric but Also Forms Multimeric Species[†]

Hugues Nury,[‡,§,||] Florence Manon,[‡,§] Bertrand Arnou,[⊥,§,#] Marc le Maire,[*,#] Eva Pebay-Peyroula,[*,‡] and Christine Ebel[*,‡]

CEA, DSV, and CNRS and Université Joseph Fourier, Institut de Biologie Structurale, 41 rue Jules Horowitz, F-38027, Grenoble, France, Institut de Biochimie et Génétique Cellulaires, CNRS UMR 5095, Université Bordeaux 2, F-33077 Bordeaux Cedex, France, and CEA, Institut de Biologie et Technologies de Saclay, and CNRS URA 2096 and Université Paris-Sud 11, LRA 17V, F-91191 Gif-sur-Yvette, France

Received June 4, 2008; Revised Manuscript Received September 25, 2008

ABSTRACT: ADP/ATP carriers (AACs) are major and essential constituents of the inner mitochondrial membrane. They drive the import of ADP and the export of newly synthesized ATP. They were described as functional dimers from the 1980s until the structures of the AAC shed doubt on this consensus. We aimed to ascertain the published biophysical data claiming that AACs are dimers and to characterize the oligomeric state of the protein before crystallization. Analytical ultracentrifugation sedimentation velocity experiments clearly show that the bovine AAC is a monomer in 3-laurylamido-*N*,*N*′-dimethylpropylaminoxide (LAPAO), whereas in Triton X-100 and reduced Triton X-100, higher molecular mass species can also be identified. Neutron scattering data for monomeric bovine AAC in LAPAO does not give definite conclusions on the association state, because the large amount of detergent and lipids is imperfectly matched by contrast methods. We discuss a possible way to integrate previously published biochemical evidence in favor of assemblies, the lack of well-defined multimers that we observe, and the information from the high-resolution structures, considering supramolecular organizations of AACs within the mitochondrial membrane.

Mitochondria are eukaryotic cell compartments responsible for the synthesis of ATP, the major energy currency of most cellular processes. Thus, adenine nucleotides have to cross the double membranes of the organelle. ADP/ATP carrier (AAC)[1] is an essential membrane protein that specifically drives the import of ADP and the export of newly synthesized ATP at the level of mitochondria inner membrane.

AAC belongs to the mitochondrial carrier family (MCF) (*1*). There are more than 45 MCF members in humans that handle a tremendous diversity of substrates implicated in mitochondrial metabolic cycles over the inner membrane. These molecules range over a large variety of size, charge, and chemical nature (for review, see ref *2*). Despite this diversity, MCF carriers possess several common features and most probably share the same fold. They are nuclear-encoded membrane proteins of approximately 300 amino acids predicted to fold as six α-helices. They are composed of three repeated modules of approximately 100 amino acids originating from ancestral duplications. Each module usually bears the signature sequence PxD/ExxK/R. AAC is the paradigm of mitochondrial carriers (for reviews see refs *3* and *4*): it is the most abundant, and it was extensively studied throughout the last four decades. It is also the first and still the only one for which a high-resolution structure is known, in complex with carboxyactractyloside (CATR), a strong inhibitor (*5*).

AAC and other mitochondrial carriers have been described as functional homodimers. Once a working hypothesis, based on the approximately equal release of ATP and uptake of ADP (see references in ref *4*) and stoichiometry of inhibitor binding (*6, 7*), the dimeric organization was fostered by substrate binding measurements

[†] This work was supported by the Centre National de la Recherche Scientifique (CNRS), the Commissariat à l'Energie Atomique (CEA), and the Université Joseph Fourier and from European Union Specific Targeted Research Project IMPS (Innovative tools for membrane protein structural proteomics). H.N. and B.A. were recipients of Ph.D. fellowships from the CEA and the Ministère de la Recherche et de la Technologie, respectively, and F.M. received a postoctoral fellowship from the program Protéines Membranaires of the Département des Sciences de la Vie, CEA.

* To whom correspondence should be addressed: (M.l.M.) tel (33) 1 6908 6243, fax (33) 1 6908 8139, e-mail marc.lemaire@cea.fr; (E.P.-P.) tel (33) 4 3878 3482, fax (33) 4 3878 5494, e-mail eva.pebay-peyroula@ibs.fr; (C.E.) tel (33) 4 3878 9570, fax (33) 4 3878 5494, e-mail christine.ebel@ibs.fr.

[‡] CEA, DSV, and CNRS and Université Joseph Fourier, Institut de Biologie Structurale.

[§] These authors contributed equally to this work.

[||] Present address: CNRS URA 2182, Channel-receptor group, Pasteur Institute, 70015 Paris, France.

[⊥] Université Bordeaux 2.

[#] CEA, Institut de Biologie et Technologies de Saclay, and CNRS URA 2096 and Université Paris-Sud 11.

[1] Abbreviations: AAC, ADP/ATP carrier; bAAC1, bovine ADP/ATP carrier isoform 1; AUC, analytical ultracentrifugation; BA, bongkrekic acid; BCA, bicinchoninic acid; BSA, bovine serum albumin; CATR, carboxyactractyloside; DDM, *n*-dodecyl β-D-maltopyranoside; EDTA, ethylenediaminetetraacetic acid; LAPAO, 3-laurylamido-*N*,*N*′-dimethylpropylaminoxide; MCF, mitochondrial carrier family; MES, 2-(*N*-morpholino)ethanesulfonic acid; MOPS, 3-(*N*-morpholino)propanesulfonic acid; SANS, small-angle neutron scattering; SE, sedimentation equilibrium; SV, sedimentation velocity; Triton X-100, α-[4-(1,1,3,3-tetramethylbutyl)phenyl]-ω-hydroxypoly(oxy-1,2-ethanediyl).

10.1021/bi801053m CCC: $40.75
Published on Web 11/04/2008

(*8*), neutron scattering (*9*) and analytical ultracentrifugation (*10*) experiments, for the bovine protein in detergent and in the membrane. With accumulating experimental evidence from bovine and yeast proteins, such as cross-linking (*11, 12*) or native electrophoresis (*13, 14*), as well as functional studies on chimeric dimers (*15*−*17*), the fact that AAC functions as a dimer was considered as well-established. The two subunits of the dimer potentially allow coordination of export of ATP and import of ADP into and out of the mitochondrial matrix. Other models implying a tetramer organization were also proposed (see ref *4*). However, the low-resolution projection map of yeast AAC (*19*) and a high-resolution structure of bovine AAC (*5*) showed that the carriers were monomeric structurally. The atomic structure of bovine AAC provided for the first time the detailed fold of the monomer, which consists of six transmembrane α-helices (*5*). The fact that the structures were monomeric brought forward the possibility that AACs were functional as monomers also (*18, 19*). On the other hand, contacts through cardiolipins defining a potential dimer were found in a second crystal form of bovine AAC (*20*). Since then, molecular mass determination in detergent (*21*), differential tagging (*22*), and the absence of negative dominance (*23*) evidenced a functional monomer for the yeast protein.

Determining monomeric/oligomeric organization of membrane proteins is difficult. In the solubilized forms, because of the presence of free detergent micelles and the fact that detergent and lipids are bound in often unknown and sometimes large amounts, the characterization of the association state is not obvious and requires rigorous thermodynamically-based techniques. Furthermore, detergent type and concentration may affect the equilibrium of association. Multimeric organization of membrane proteins is widely and even sometimes hotly debated for a number of proteins in the attempt to correlate organization with regulatory aspects and to define the role that quaternary structure plays in the basic function (see, for example, refs *24*−*28*).

In this work, we present analytical ultracentrifugation (AUC) and small-angle neutron scattering (SANS) results. The solubilized and purified proteins are monomers, but some indications for multimeric assemblies exist. We discuss a possible way to integrate published biochemical evidence in favor of assemblies, the absence of well-defined multimers in our samples, and the information from the high-resolution structures by considering supramolecular organizations of AACs within the mitochondrial membrane.

MATERIALS AND METHODS

Chemicals. CATR was purchased from Sigma, bongkrekic acid (BA) was purified according to Lauquin and Vignais (*29*), and α-[4-(1,1,3,3-tetramethylbutyl)phenyl]-ω-hydroxy-poly(oxy-1,2-ethanediyl) (Triton X-100) was from Sigma. Reduced Triton X-100 is also known as hydrogenated Triton X-100. In this form, the benzene moiety is fully hydrogenated to a cyclohexane derivative. Reduced Triton X-100 was purchased from Aldrich. *n*-Dodecyl β-D-maltopyranoside (DDM) was from Anatrace; 3-laurylamido-*N*,*N*′-dimethylpropylaminoxide (LAPAO) was synthesized as previously described (*8*); and Aminoxid WS-35 was from Goldschmidt, Le Chesnay France.

Quantifications. Lipids were quantified with a colorimetric assay for the total phosphorus amount (*30*), and proteins were quantified by the Lowry or bicinchoninic acid (BCA) method with bovine serum albumin (BSA) as a standard. The two methods provided similar results when the same standard was used, BCA being more sensitive and with more stable coloring. Total Triton X-100 was estimated with an extinction coefficient at 280 nm of 2.24 mg/cm^2.

A. Purification of the bAAC1−*CATR Complex and Related Lipid Samples in the Presence of LAPAO for Sedimentation Velocity and SANS Experiments.* Bovine mitochondria were first incubated for 10 min at 0 °C at a concentration of 4 mg of total mitochondrial proteins/mL in the presence of either CATR (20 μM) or BA (20 μM) in a medium made up of 0.27 M sucrose supplemented with 10 mM Tris-HCl, final pH 7.3, or with 10 mM MES, final pH 6.6, respectively. ADP/ATP carrier was extracted from mitochondria with 2% LAPAO and purified by hydroxyapatite chromatography as described earlier (*31*). The CATR−carrier complex was then chromatographed on an AcA 202 size-exclusion column in a medium consisting of 5 mM NaCl, 10 mM Tris, 1 mM EDTA, and 0.02% (w/v) LAPAO, final pH 7.3. The recovered ADP/ATP carrier fraction was then divided into two parts, one of which was incubated in the presence of Bio-beads to lower the detergent-to-protein ratio (*31*). Both samples were then concentrated on Amicon Ultra-4 30K filtration units (Millipore) to about 3 mg/mL. Solvent exchange was achieved for half of each concentrated fraction by overnight dialysis against the same buffer but prepared in D_2O. LAPAO and membrane lipids present in the preparations of bAAC1 were extracted with chloroform/methanol (2/1 v/v) from freeze-dried samples, purified as described above, and subjected or not to Bio-beads treatment. The soluble fractions were recovered by centrifugation and dried under a nitrogen stream at room temperature. The resulting solid residues were dissolved in H_2O or in D_2O in final volumes equal to that of the corresponding protein samples.

B. Ammonix-Solubilized bAAC1 for Sedimentation Equilibrium Experiments. Samples were prepared as in ref *32*. Buffer composition for bAAC/Aminoxid WS 35 was 0.1 M Na_2SO_4, 10 mM MOPS (pH 7.4), and 5 mg/mL Aminoxid WS 35.

C. Purification of bAAC1−*CATR Complex in the Presence of Triton X-100 for Sedimentation Velocity Experiments According to Hackenberg and Klingenberg Protocol.* The complex was solubilized and isolated in the presence of Triton X-100 as described earlier (*10*). The purified protein was concentrated to approximately 8 mg/mL. Excess Triton X-100 was removed by centrifugation on a 5−15% sucrose gradient for 38 h at 40 000 rpm at 4 °C in a Beckman Ti70 rotor. The recovered protein fraction (0.4 mg/mL protein, 2.5 mg/mL Triton X-100, 0.4 g of lipid/g of protein) was divided into two parts, which were dialyzed against a buffer consisting of 0.1 M NaCl, 10 mM MOPS, and 0.5 mM EDTA, pH 7.2, prepared with H_2O or with D_2O.

D. Purification of bAAC1−*CATR and bAAC1*−*BA Complexes without Elimination of Excess Detergent in the Presence of Triton X-100 or Reduced Triton X-100.* Bovine mitochondria pretreated with CATR or BA were solubilized with 3% (w/v) Triton X-100 or reduced Triton X-100. Isolation of the CATR− and BA−carrier complexes was

carried out as described for LAPAO but with Triton X-100 or reduced Triton X-100 instead of LAPAO. The purified fractions recovered from the chromatographic steps (0.1 mg of protein/mL) were subjected to solvent exchange by size-exclusion chromatography on Bio-Gel P6DG (Bio-Rad) columns equilibrated in a buffer made up of 5 mM NaCl, 10 mM Tris, 1 mM EDTA, and 0.02% (w/v) reduced Triton X-100, final pH 7.3, prepared with either H_2O or D_2O. The pass-through fractions were used for sedimentation velocity (SV) experiments without any further treatment.

Neutron Scattering Experiments. Experiments were performed on beamline D22 of the Institut Laue Langevin (Grenoble) (http://www.ill.fr/YellowBook/D22/). Scattering data were recorded at 4 °C for 1−5 h in quartz cells of 1 mm. The sample to detector distance was 4 or 5.6 m, wavelength 10 Å. A corrective mask was applied on the detector before radial integration of the data, normalization, and analysis following standard protocols. The radii of gyration of scattering contrast, R_g, of the samples were determined from the scattered intensity, $I(q)$, by applying the Guinier approximation, which is valid for a q range in which $(R_g q)^2 \sim 1$: (*33*)

$$I(q) = I(0) \exp(-R_g^2 q^2/3) \quad (1)$$

If the sample is polydisperse, the $I(0)$ and R_g^2 values represent number averages. $I(0)$ can be expressed as

$$I(0) = \sum (1/N_A) c_i M_i (\partial \rho_N / \partial c_i)_\mu^2 \quad (2)$$

where N_A is Avogadro's number, c_i (grams per milliliter) is the concentration, M_i (grams per mole) is the molar mass, and $(\partial\rho_N/\partial c_i)_\mu$ (centimeters per gram) is the neutron scattering length density increment, which depends on particle and solvent composition (*34*). This term is null when the solvent contains ≈15% D_2O (matching point) for detergent/lipid components. When the protein solutions are measured at the matching point of detergent/lipid, $I(0)$ relates to the protein component within the complexes.

Samples of AAC that were not incubated with Bio-beads displayed a peak of interference at ≈ 0.06 $Å^{-1}$, most probably related to significant particle−particle correlation of the lipid/detergent micelles in large excess. This prohibits analysis of the scattering curves in terms of protein molecular weight. Only the samples after incubation with Bio-beads were used for analysis. The matching point was determined with LAPAO−lipid mixtures mimicking the protein samples (see above) containing known amounts of D_2O. The Guinier analysis was made on mixtures of bAAC1 protein samples at 15% D_2O corresponding to the matching point of the LAPAO−lipid mixture. For particle mass determination, the protein concentration was quantified by amino acid analysis.

Analytical Ultracentrifugation Experiments. They were typically performed in a Beckman XLI ultracentrifuge using an ANTi-50 rotor. Sedimentation velocity were at 42 000 rpm at 10 °C (LAPAO and bAAC1 in LAPAO in the presence of H_2O and D_2O solvents) or 20 °C (LAPAO−lipid mixtures in the presence of H_2O and D_2O solvents and bAAC1 with Triton X-100) or at 60 000 rpm and 20 °C (Triton X-100 in H_2O and D_2O solvents), in double-sector cells with an optical path of 3 or 12 mm, with absorbency typically at 278 nm and interference optics. The sedimentation equilibrium experiments were followed at 280 nm in a Beckman Model E ultracentrifuge, at 30 000 rpm and 20 °C as described previously (*35*) for bAAC1 in Aminoxid WS 35.

Background for AUC Analysis and Interpretation. The transport of noninteracting species in solution is related to the sedimentation (s) and diffusion (D) coefficients. For an ideal solution, the relationships between s and D and the molecule characteristics, that is, hydrodynamic radius (R_H) and buoyant molecular mass (M_B), follow Svedberg and Stokes−Einstein equations:

$$s = M_B/(N_A 6\pi\eta R_H) \quad (3)$$

$$D = RT/(N_A 6\pi\eta R_H) \quad (4)$$

where N_A is Avogadro's number. For the complex composed of protein, detergent, and lipids, M_B can be written

$$M_B = M^*(1 - \bar{v}^* \rho) = M_p(1 - \bar{v}_p\rho) + M_p B_d(1 - \bar{v}_d\rho) + M_p B_l(1 - \bar{v}_l\rho) \quad (5)$$

An asterisk designates the whole protein particle (detergent−lipid−protein complex). Index p is for protein, d is for detergent, and l is for lipid, or d+l when detergent and lipids are considered as a whole. M is the molecular mass, $\bar{v}$ is the partial specific volume, and B is the amount of detergent and/or lipid bound to the protein in grams per gram. R_H can be related to the frictional ratio f/f_0 and the minimum radius corresponding to the volume of the particle, R_0:

$$R_H = (f/f_0)R_0 \quad (6)$$

$$(4\pi/3)R_0^3 = (1/N_A)(M_p\bar{v}_p + M_p B_d \bar{v}_d + M_p B_l \bar{v}_l) \quad (7)$$

From eqs 3 and 5, SV experiments performed in D_2O and H_2O solvents (of different densities) allow the determination of the partial specific volume of sedimenting particles, if it is assumed that their composition and shape do not change (s_H/s_D method) (*36, 37*), which was used for LAPAO, LAPAO−lipid, and Triton X-100 micelles. We used eqs 3 and 5−7 to determine ($\bar{v}_{d+l}$, B_{d+l}) solutions corresponding to s, for given values of M_p (monomer and dimer) and f/f_0 for bAAC1 in a procedure described in the Results section.

Analysis of AUC Data. Analysis of SV data was carried out with Sedfit and Sedphat, which can simultaneously analyze different sets of data (available free at www.analyticalultracentrifugation.com). These software programs use numerical solutions of the Lamm transport equation to consider noninteracting species. The analysis also uses systematic noise evaluation. Analysis was done in terms of noninteracting species [allowing the determination of s and (for homogeneous samples) of D, and thus M_B, for each species] or in terms of a continuous distribution $c(s)$ of sedimentation coefficients (*38*). The $c(s)$ method deconvolutes the effects of diffusion broadening, which results in high-resolution sedimentation coefficient distributions. This is done by assuming a relationship between the sedimentation and diffusion coefficients s and D, which determine the sedimentation process for a given particle, through reasonable values of $\bar{v}$ (intermediate between that of the detergent and the protein for a membrane protein) and frictional ratio, f/f_0. Typically $f/f_0 = 1.25$ corresponds to globular compact particles (*39*). These values are the same for all the particles (typically 200) considered in the distribution. The two types of analysis also give, for each species, the corresponding

Table 1: Overview of Experiments on Bovine AAC

detergent	protocol[a]	technique[b]	interpretation	published conclusions
LAPAO 0.02%	sp/concn/dia	AUC (SV)	monomer	
LAPAO 0.02%	sp/concn/dia	SANS	monomer or dimer	dimer (*9*)
Aminoxid WS35 0.05%	sp/concn/dia	AUC (SE)	monomer	
Triton X-100 0.02%	sp/concn/sucr/dia	AUC (SV)	monomer + multimers	dimer(*10*)
Triton X-100 0.02%	sp	AUC (SV)	monomer or dimer	
reduced Triton X-100 0.02%	sp	AUC (SV)	monomer + multimers	

[a] sp, standard protocol consisting of solubilization of the membrane followed by concentration, hydroxyapatite, and gel-filtration steps; concn, concentration step with ultrafiltration; dia, dialysis; sucr, sucrose gradient. For details of the purification protocols, see the Materials and Methods section.. [b] AUC, analytical ultracentrifugation; SV, sedimentation velocity; SANS, small-angle neutron scattering; SE, sedimentation equilibrium; SEC, size-exclusion chromatography.

signal in absorbance (A) or fringe shift (J). A and J can be analyzed in terms of concentration or composition, according to the Beer−Lambert law and

$$J = \Sigma[(\partial n/\partial c)/\lambda]lc \quad (8)$$

$\partial n/\partial c$ is the refractive index increment, λ is the laser wavelength, l is the optical path length, and c is the concentration. In the condition of sedimentation equilibrium, for a homogeneous protein sample and when detergent does not absorb, the plot of ln $A(r)$ as a function of r^2, where $A(r)$ is the absorbance at radial position r, is a straight line whose slope gives M_B. With ω the angular velocity:

$$\mathrm{d}\ln[A(r)]/\mathrm{d}r^2 = \omega^2 M_B/2RT \quad (9)$$

Recent reviews, both general and focused on membrane proteins, describing AUC background and analysis can be found in refs *37*, *40*, and *41*.

Numerical Values for AUC. Solvent viscosities were measured with an AMVn (Anton Paar, Graz, Austria) apparatus: 1.303 and 1.647 mPa/s for H_2O and D_2O solvents for bAAC1 in LAPAO SV experiments at 10 °C; 1.03 and 1.23 mPa/s for H_2O and D_2O solvents for bAAC in Triton X-100 SV experiments at 20 °C; 1.015 and 1.262 mPa/s for H_2O and D_2O solvents for bAAC1 in reduced Triton X-100 SV experiments at 20 °C. Densities (ρ) were measured with a DMA 5000 (Anton Paar) apparatus or calculated according to composition: 1.001 and 1.104 g/mL for H_2O and D_2O solvents for LAPAO SV experiments at 10 °C; 1.003 and 1.108 g/mL for H_2O and D_2O solvents for Triton X-100 SV experiments at 20 °C; and 0.999 and 1.104 g/mL for H_2O and D_2O solvents for reduced Triton X-100 SV experiments at 20 °C. Densities for SE experiments in the presence of $H_2{}^{18}O$ are reported in Figure 3.

The molecular masses of the transporter from beef and yeast are 32.8 and 36.5 kDa. We consider, for bAAC1, the extinction coefficients $E_{0.1\%} = 1.39$ mg/cm^2, $\partial n/\partial c = 0.186$ mL/g, and $\bar{v} = 0.741$ mL/g at 10 °C or 0.745 at 20 °C calculated from composition by use of Sednterp (available free at http://www.jphilo.mailway.com). The $\bar{v}$ value of Aminoxid WS 35 was calculated to be 1.061 mL/g according to ref *42*. The $\bar{v}$ values of LAPAO, Triton X-100, and reduced Triton X-100 were estimated from SV in hydrogenated and deuterated solvents (s_H/s_D method): 1.002 ± 0.001, 0.92 ± 0.03, and 0.93 ± 0.1 mL/g, respectively. We measured similar values using density: 0.94 ± 0.02 and 0.921 ± 0.004 mL/g for Triton X-100 and reduced Triton X-100, respectively. For further calculations, we used the following values: for Triton X-100, $\bar{v} = 0.924$ mL/g; for reduced Triton X-100, $\bar{v}$ in the range 0.92−0.94 mL/g; and for lipids, 0.981 mL/g reported for egg yolk phosphatidylserine (*43*).

The extinction coefficients of LAPAO, Triton X-100, and reduced Triton X-100 were experimentally determined in the ultracentrifuge as 0.009, 2.31, and 0.078 mg/cm^2, respectively. We considered for $\partial n/\partial c$ the values of 0.143 g/mL for DDM (*44*), 0.134 g/mL for LAPAO−lipid mixtures [which is chosen arbitrarily the same as the value for $C_{12}E_8$ (*45*)], and 0.097 and 0.115 g/mL for Triton X-100 and reduced Triton X-100, the latter being experimentally determined from the ratio J/c in the ultracentrifuge.

RESULTS

An overview of experiments, including the detergent used as well as experimental techniques, is given in Table 1. Our experiments cover a range of purification protocols and detergent conditions, some of which correspond to former publications by different laboratories. In sedimentation velocity experiments, the different species in solution are expected to sediment at different rates. The technique is thus particularly appropriate to qualify sample homogeneity and discriminate the behavior of the different species in solution. The sedimentation coefficients, s, depend on particle buoyant molar mass and hydrodynamic radius (eq 3). These are determined for the particle not only by association state but also by detergent and lipid binding. In addition, buoyant molar mass depends on solvent density (eq 5). There are different ways to decipher the intrinsic complexity of membrane protein solution systems. First, we varied the density of the solvent (by substituting H_2O with D_2O). The detergents that are studied here have densities close to 1, which represents a favorable case (*36*): the buoyant molar mass (and thus s) is strongly affected when the solvent density is modified. For example, flotation is observed in D_2O when the solvent density exceeds that of the particle (the detergent micelle or protein complex). Second, we use different optical systems: absorbance and interference, which give indications on complex composition because detergent, lipids, and protein do not have the same extinction coefficients, the easier case being when detergent does not absorb (Beer−Lambert law and eq 8). Interpretation of the s values requires knowledge of the hydrodynamic radius, R_H, of the complex, which can be obtained by two ways: in the particular case of homogeneous systems (such as AAC in LAPAO, see below), the analysis of boundary spreading provides an estimate of the diffusion coefficient and thus R_H (eq 4); or in the general case, R_H may be estimated from the composition (the minimum possible value is easily

calculated, and the frictional ratio that links it to R_H has a restricted range of possible values) (eqs 6 and 7). New protocols of analysis of H_2O/D_2O data, using graphical representation, were here defined (see below) to account for the experimental possibilities of detergent/lipid binding and respond to the question: are the sedimentation coefficients measured in H_2O/D_2O compatible with a given association state? Sedimentation equilibrium in H_2O/D_2O mixtures in principle can determine more easily the buoyant masses [SE profiles do not depend on R_H values (eq 9)]. But since SE does not deconvolute the contributions of different species, interpretations of the measurements are easy only for homogeneous samples with nonabsorbing solvent (such as AAC in Aminoxid WS35, see below). SANS intensity, for diluted noninteracting systems, is the sum of the contribution of the different particles in solution, including detergent−lipid micelles. H_2O/D_2O solvent mixtures can be used in principle to match the signal of the detergent + lipid component. The data at low angle (eq 1) can be then used to determine, in the Guinier approximation, values for the radius of gyration of scattering density contrast (R_g) and the forward intensity $I(0)$, representing the protein within the complex. For homogeneous protein complexes, the molar mass of the protein within the complex can be calculated from $I(0)$ (eq 2).

bAAC1 in LAPAO Is a Monomer under the Crystallization Conditions. A. Principle. The association state of bAAC1 purified in LAPAO, as for crystallization (*31*), was first investigated by sedimentation velocity (SV) analytical ultracentrifugation. The protein solution used for crystallization assays contains unusually high amounts of detergent and lipid molecules, even after incubation in the presence of Bio-beads. We measured in the whole sample a molar detergent/protein ratio of 1000 (*31*) and lipid/protein ratios of 170 (this work). In order to deal with the excess of lipids and detergents, we performed SV experiments in two buffers of different densities, with H_2O and D_2O. Indeed, LAPAO−lipid micelles are expected to float in D_2O buffer and to neither float nor sediment in H_2O buffer.

B. Sedimentation of LAPAO Micelles. LAPAO at approximately 5% [all percentages are weight per volume (w/v) unless stated] in H_2O and D_2O buffers displays a weak flotation in SV experiments (sedimentation coefficient $s = -0.005 \pm 0.004$ S in H_2O buffer and $s = -0.21 \pm 0.003$ S in D_2O buffer at 10 °C; data not shown). The two data sets were modeled together, the fringe shift number corresponding to LAPAO concentration being fixed. It led to a partial specific volume for the detergent $\bar{v}_d = 1.002$ mL/g, a value close to the previously reported one $\bar{v}_d = 1.067$ mL/g (*46*). The *s* values are compatible with globular LAPAO micelles composed of 125 monomers (supplier information).

C. Sedimentation of LAPAO−Lipid Mixed Micelles. Figure 1a,b shows the sedimentation of LAPAO−lipid mixtures. Sample preparation was designed in such a way that the composition mimics that in the protein samples. The samples exhibit significant absorbency and, near the meniscus in D_2O buffer, an optical artifact (this artifact is actually seen in all the samples containing lipids). Therefore, this region is excluded in the analysis. LAPAO−lipid mixtures in H_2O buffer do not sediment nor float significantly. In D_2O buffer they exhibit a weak flotation ($s = -0.75$ S at 20 °C corresponding to −0.56 S at 10 °C). The behavior of

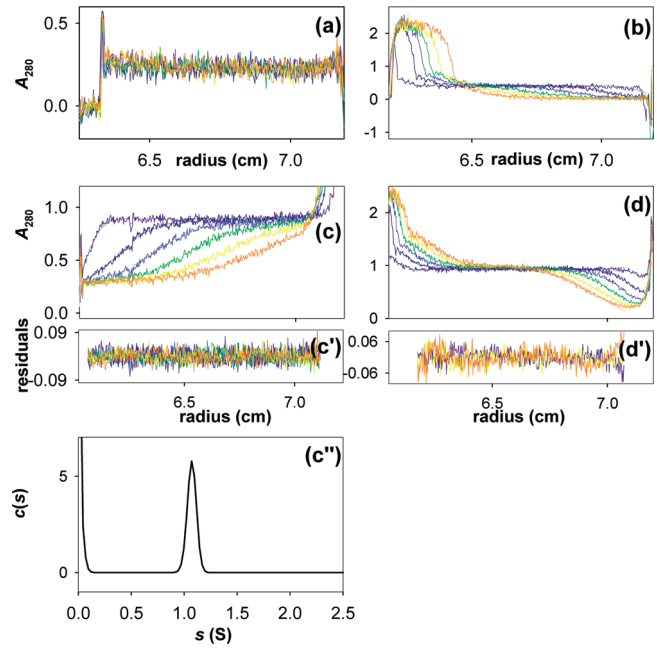

FIGURE 1: Sedimentation velocity experiments of LAPAO−lipid mixtures and bAAC1 in LAPAO. Sedimentation velocity profiles at 42 000 rpm, in 3 mm cells, at 20 °C of LAPAO−lipid mixtures in (a) H_2O or (b) D_2O and of protein samples at 10 °C in (c) H_2O or (d) D_2O are shown. Experimental and fitted data are superimposed in panels c and d. (c′, c″) Residuals and *c*(*s*) analysis of the H_2O data. (d′) Residuals of the analysis in terms of one component species for the D_2O data. Samples are obtained following incubation with Bio-beads. LAPAO−lipid mixtures were prepared in such a way that their concentrations mimic the corresponding concentrations in the protein sample. Protein concentration is approximately 3 mg/mL. For clarity reasons, only six curves were drawn for each experiment, for a total time of 18 h sedimentation.

mixtures treated with Bio-beads is similar (at 20 °C, *s* is close to 0 in H_2O buffer; $s = -1.07$ S in D_2O buffer). These results are compatible with a partial specific volume $\bar{v}_{d+l}$ close to 1.00 mL/g for mixed LAPAO−lipid mixed micelles.

D. Sedimentation of bAAC1−LAPAO Samples. Figure 1c shows the sedimentation of bAAC1 in H_2O buffer and the analysis in term of particle distribution. The data are in agreement with a single species and the analysis in terms of one type of sedimenting particle leads to $s = 1.06 \pm 0.01$ S and a diffusion coefficient $D = 4.2 \pm 0.2\ 10^{-7}$ cm^2/s at 10 °C. The micelles without protein do not sediment and contribute as a baseline to the absorbency and interference signals (latter not shown). Differences between Bio-bead-incubated samples and untreated samples are minor in terms of *s*, *D*, and number of interference fringes over absorbency (J/A_{278} ratio). The J/A_{278} ratio of the protein complex is related to detergent plus lipid over protein ratio. All components contribute to the interference signal, while absorbency accounts only for the protein part. From this ratio, we determine $J/c = 7.23$ [fringes (mg of protein)$^{-1}$ mL, for a 1 cm optical path]. For pure protein, J/c is 2.76; the sample therefore exhibits an excess of 4.47 fringes, which gives an amount of bound detergent and lipid B_{d+l} of 1.9 ± 0.3 g/g (see the Materials and Methods section).

Profiles of experiments in D_2O buffer show that both the protein complex and the LAPAO−lipid micelles float together weakly (Figure 1d). We were not able to separate the two boundaries. We therefore obtain only an estimation of the sedimentation coefficient within the range −0.2 to

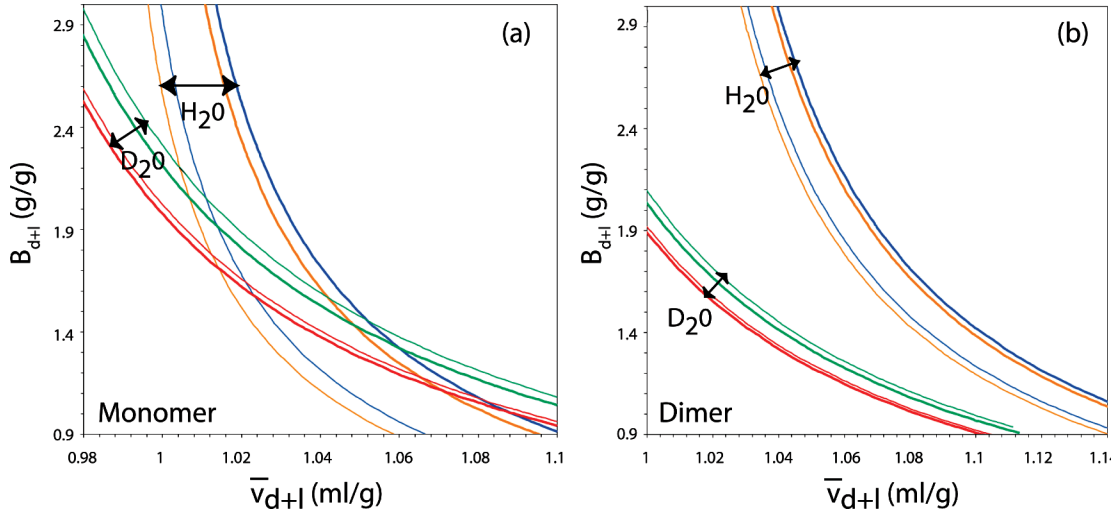

FIGURE 2: Compatibility of SV experiments in H_2O and D_2O considering (a) a monomeric model or (b) a dimeric model. The implicit $B_{d+1} = f(\bar{v}_{d+1})$ function is drawn for f/f_0 ratios of 1.25 (bold lines) and 1.5 (thin lines), for experimental s values in H_2O (blue and yellow lines, corresponding to lower and higher values within the uncertainty range) and in D_2O (green and red lines). The existence of an intersection area between the curves in H_2O and those in D_2O for the monomer model (panel a) demonstrates that this hypothesis is correct.

−0.1 S at 10 °C for the protein complex, which is the main absorbing species.

E. The Protein Is Monomeric. Three different arguments support a monomeric protein within the complex. First, the combination of s and D determined in H_2O buffer gives, for an amount of bound detergent and lipid of $B_{d+1} = 1.9$ g/g (when $\bar{v}_{d+1} = 1$ mL/g is used), a protein molecular mass of 23 ± 1 kDa, a value even lower than the protein molecular mass deduced from the knowledge of the protein sequence (about 32 kDa). The buoyant molecular mass obtained from this s and D combination is 6 ± 0.3 kDa. From the same hypothesis, we calculate buoyant molecular masses of 8.4 kDa for a monomer and 16.8 kDa for a dimer. Second, the experimental D value corresponds to a hydrodynamic radius of 38 ± 2 Å. The calculated values for a globular monomeric or dimeric particle (same B_{d+1} and $\bar{v}_{d+1}$; $f/f_0 = 1.25$) are 41 and 52 Å, respectively. These two arguments support the monomer hypothesis. It could be argued, however, that analytical ultracentrifugation bears impreciseness on the diffusion coefficient D. The third argument therefore lies in the combined analysis of the robust values of the sedimentation coefficients s determined in H_2O and D_2O buffers. The Svedberg equation (eqs 3, 5, and 7, Materials and Methods section) shows that s depends on a number of parameters. The protein mass can be only that of a monomer or a dimer, trimer,..., and the frictional ratio lies within a narrow range, except for an unfolded or very anisotropic particle (*39*). On the contrary, the amount of bound detergent plus lipid (B_{d+1}) and their partial specific volume ($\bar{v}_{d+1}$) are free parameters, which cannot be solved separately in unique solvent conditions (constraining viscosity and density). If the oligomeric state is appropriately chosen, a unique pair of (B_{d+1}, $\bar{v}_{d+1}$) values must account for sedimentation in H_2O and D_2O buffers. Figure 2a shows the (B_{d+1}, $\bar{v}_{d+1}$) solutions, for the experimental s values in both buffers, for a monomeric protein and frictional ratio f/f_0 between 1.25 and 1.5. The imprecision of s was also considered. A common region is defined within the intersection of the set of curves built for H_2O buffer and the set built for D_2O buffer. This region corresponds to a partial specific volume ($\bar{v}_{d+1}$) value between 1.01 and 1.06 mL/g and an amount of bound detergent plus lipids of 1.3−2.2 g/g, in good agreement with the independent analysis of LAPAO−lipid sedimentation and J/A_{278} values for the protein complex in H_2O buffer. In the dimeric hypothesis (Figure 2b), there is no intersection between the two sets of curves for realistic $\bar{v}_{d+1}$ values. This hypothesis is therefore rejected. Our results thus clearly show that the protein is monomeric during the late stages of its purification and under the crystallization conditions.

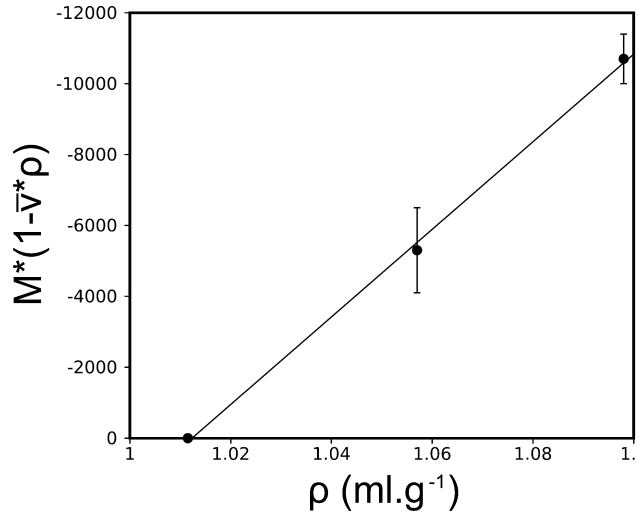

FIGURE 3: Sedimentation equilibrium of bAAC1 in Aminoxid WS35. The parameter $M^*(1 - \bar{v}^*\rho)$ is plotted against solvent density, which was changed by addition of $H_2{}^{18}O$. Each point, except in H_2O, is the average of three determinations.

F. SANS on bAAC1 in LAPAO Are Difficult to Analyze. We performed small-angle neutron scattering (SANS) experiments with the same samples used for SV experiments. Sample prepared without the Bio-beads step showed interparticle correlation peaks, and we focused on the samples treated with Bio-beads. The key point of SANS is that tuning the deuterium amount of the solvent allows us to match the mean scattering contribution of a chosen component. This is of particular interest for multicomponent systems such as membrane proteins for which detergents and/or lipids can be matched out (*47, 48*). In principle, it enables us to measure the parameters of the sole protein within a protein−detergent

complex. The matching point of the LAPAO−lipid mixture (mimicking the composition in the protein sample) is determined by plotting the square root of the normalized forward scattered intensity $I(0)$ against the D_2O/H_2O ratio for the LAPAO−lipid mixture. This yields a straight line, indicating that the contribution of LAPAO and lipids was null at 15% D_2O (see Supporting Information Figure SI-1). (1) bAAC1-LAPAO samples scattering is measured at the matching point of 15% D_2O (see Supporting Information Figure SI-2 for a typical Guinier curve). The Guinier approximation leads to experimental values of $R_g = 30$ Å for the gyration radius [the same as found previously by Block et al. (*9*) in 1982] and of $M = 44$ kDa for the particle mass. Calculated gyration radii from crystallographic models are 20.4 and 30.4 Å for the monomer and dimer proteins. The molecular mass from SANS falls between the values for a monomer (32.8 kDa) and a dimer (65.6 kDa). However, bAAC1 in this sample is clearly a monomer from the SV results.

Our samples are similar to the ones used by Block et al. (*9*) in 1982, and the experimental data also look similar. While the authors concluded the protein was dimeric, our results put forward the difficulty of interpretation of scattering curves from a monomeric protein. The reason for this discrepancy lies in the complexity of the bAAC1−LAPAO samples, which contain a huge amount of detergent and lipid, as stated above. Therefore, in practice it is not possible to properly match the scattering contribution of such abundant species and to draw definitive conclusions on the sole basis of SANS.

bAAC in Aminoxid WS35 Is a Monomer. Figure 3 shows measurements of buoyant molecular mass, $M^*(1 - \bar{v}^*\rho)$, of the protein−detergent complex obtained by sedimentation equilibrium (SE) of bAAC in the presence of Aminoxid WS35. This detergent is similar to LAPAO (*32*) but has alkyl chain lengths ranging from 12 to 18 carbon atoms, the average length being 14. Experiments are performed at various solvent densities, obtained by addition of $H_2{}^{18}O$. In H_2O there is no sedimentation, while at increased densities the particle is floating, giving rise to negative values of $M^*(1 - \bar{v}^*\rho)$. Given the partial specific volumes of the protein and of the detergent, one can then calculate M^* $\bar{v}^*$(slope of the line). It leads to a protein mass value $M = 28 \pm 7$ kDa, corresponding to a monomer and a detergent binding ratio of about 3.5 g/g of protein. It should be noted that this method is precise for protein mass determination but is not very precise for detergent binding determination (*49*), in particular when $\bar{v}^*$ is not precisely known. However, the obtained value for detergent binding is reasonable when compared with LAPAO binding or the 13 M (tridecyl β-maltoside) binding to yAAC (isoform 3) of 3 g/g (*21*).

bAAC in Triton X-100 Is a Mixture of Different Multimeric Species following the Hackenberg and Klingenberg Protocol. Our protocol for sample preparation and SV data record is designed here to be essentially similar to that given by Hackenberg and Klingenberg (*10*), who reported the presence of a dimer as a single species of bAAC in this detergent. bAAC solubilized in Triton X-100 is centrifuged on a sucrose gradient in order to remove the excess mixed detergent/lipid micelles and then dialyzed to eliminate sucrose. Sedimentation velocity profiles obtained at 20 °C, at 278 nm and by use of interference optics, are analyzed in terms of continuous

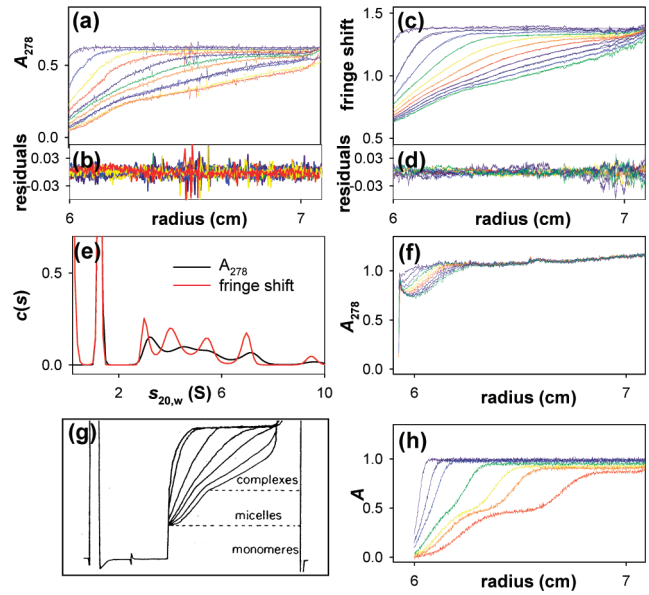

FIGURE 4: Sedimentation velocity experiments of bAAC1 in Triton X-100. (a) Superimposition of selected experimental sedimentation profiles obtained at 278 nm during 4 h at 42 000 rpm, at 20 °C, in 3 mm cells and of their modeled profiles with the $c(s)$ analysis. (b) Corresponding residuals. (c, d) Same as panels a and b for data acquired with interference optics. (e) Result of the $c(s)$ analysis for data from panel a (black line) and panel c (red line). (f) Raw absorbency data obtained under the same conditions after dialysis with deuterated solvent. (g) Experimental profiles (at 11, 36, 59, 86, 109, and 156 min at 52 000 rpm, 23 °C). Reprinted with permission from ref *10*; copyright 1980 American Chemical Society. (h) Simulated profiles (same angular velocity, at 10, 20, 30, 60, 90, 110, and 160 min) for Triton X-100 micelles and a protein complex with $s = 1.3$ S and $D = 6\ 10^{-7}$ cm^2/s given for bAAC1 by Hackenberg and Klingenberg (*10*). The clear difference in the shape of the protein complex boundary in panels g and h is explained by the heterogeneity of the sample in panel g.

distributions of sedimentation coefficients $c(s)$, both revealing the same complex features (Figure 4). Experiments done with samples diluted two and three times in a solvent without detergent gave $c(s)$ curves of the same appearance except for the relative intensity of the peak at $s = 1.3 \pm 0.1$ S (data not shown).

This peak corresponds to the Triton X-100 micelles. In H_2O buffer, Triton X-100 at 0.5 mg/mL sediments at $s = 1.22$ S (similar to $s = 1.3$ S given previously (*10*)), while in D_2O buffer, the micelles float at $s = -0.3$ S (data not shown). The movement of the detergent monomer is not detected, corresponding to s smaller than 0.2 S in H_2O buffer and 0.01 S in D_2O buffer. The absorbance corresponding to the monomer, $A_{278,1cm} = 0.35$, corresponds to a critical micelle concentration (cmc) of 0.16 mg/mL (Anatrace value is 0.15 mg/mL). Combined analysis of the sedimentation coefficients of the Triton X-100 micelles in the two buffers gives $\bar{v}_d = 0.92 \pm 0.035$ mL/g, close to the value we determine by density ($\bar{v}_d = 0.94 \pm 0.02$ mL/g) and to the previous value (*10*) ($\bar{v}_d = 0.908$ mL/g). For pure detergent micelles, we measure in the ultracentrifuge a ratio of $J/A_{278} = 0.7$ and, for the 1.3 S peak in the bAAC samples, a slightly larger ratio of $J/A_{278} = 1.1 \pm 0.2$, which may be accounted for by the presence of lipids. When the values A_{278} and $E_{0.1\%} = 2.3$ (determined experimentally) are considered, the free Triton X-100 micelle concentration in the sample after sucrose gradient and dialysis is 0.4 mg/mL, that is, a total detergent concentration only about 4 times the cmc.

Table 2: Analysis of the Main or Smallest Complex of bAAC1 in LAPAO, Triton X-100, and Reduced X-100 in H_2O and D_2O Solvents[a]

	SV data[b]	monomer hypothesis	dimer hypothesis	conclusion
		LAPAO		
$\bar{v}_d = 1.00$ $B_{d+1} = 1.9 \pm 0.3$[c]	$s_H = 1.06 \pm 0.02$ $s_D = -0.15 \pm 0.005$	$\bar{v}_{d+1} = 1.04 \pm 0.03$ $B_{d+1} = 1.6 \pm 0.6$	$\bar{v}_{d+1} > 1.2$ $B_{d+1} < 0.6$	monomer
		Triton X-100 after Sucrose Gradient		
$\bar{v}_d = 0.92$ $B_{d+1} = 2.5$;[c] $B_l = 0.4$;[d] $B_d = 1.5$;[e] $B_l = 0.25$[e]	$s_H = 3 \pm 0.3$[f] $s_D = 0.9 \pm 0.2$[f]	$\bar{v}_{d+1} = 0.91 \pm 0.03$ $B_{d+1} = 2.2 \pm 2.2$	$\bar{v}_{d+1} = 0.99 \pm 0.03$ $B_{d+1} = 1.1 \pm 0.7$	monomer
		Triton X-100, Quick Purification		
$\bar{v}_d = 0.92$	$s_H = 3-4$ $s_D = 0.55-1.3$	$\bar{v}_{d+1} = 0.89 \pm 0.035$ $B_{d+1} = 4.5 \pm 3.5$	$\bar{v}_{d+1} = 0.96 \pm 0.05$ $B_{d+1} = 2 \pm 1.5$	no conclusion
		Reduced Triton X-100, Quick Purification		
$\bar{v}_d = 0.93 \pm 0.01$ $B_l = 1.2$[d]	$s_H = 2.0 \pm 0.1$[f] $s_D = -0.4 \pm 0.4$[f]	$\bar{v}_{d+1} = 0.975 \pm 0.02$ $B_{d+1} = 4.5 \pm 2$	$\bar{v}_{d+1} = 1.06 \pm 0.05$ $B_{d+1} = 1.4 \pm 0.4$	monomer

[a] $\bar{v}$ is given in milliliters per gram, B is given in grams per gram, and s_H and s_D are given in Svedbergs. Analyses are made with frictional ratio in the range 1.25−1.5. Conclusions are based on the fact that $\bar{v}_{d+1}$ should reasonably be between $\bar{v}_d$ and $\bar{v}_l \sim 1$ mL/g and reflect the B_d/B_l ratio when estimated, and B_{d+1} should be compatible with estimated values given in the left column. [b] Buffer densities and viscosities are reported in the Materials and Methods section [c] From J/A_{278} in SV. [d] From chemical analysis. [e] From ref *10*. [f] s_H is for the smallest complex; s_D is a mean value for all complexes.

The main distribution for bAAC is between 2.7 and 8 S, with peaks at 3.1 and 7 S and two additional peaks (Figure 4e). There is also a species at approximately 9.5 S and a small amount of aggregates. We evaluate a mean s value of 5 S, close to the value of 3.9 S published in 1980. It is likely that the sample of Hackenberg and Klingenberg (*10*) also consisted of a mixture of various oligomers. In Figure 4a,c, the last sedimentation profiles correspond in terms of $\omega^2 t$ values to that in Figure 6S from ref *10*, which is reprinted in Figure 4g for comparison. The general appearance of boundaries in Figure 4g is rather similar to ours. In the previous work the putative dimer was characterized as $s = 3.9$ S and $D = 3.4 \times 10^{-7}$ cm^2/s. We show in Figure 4h simulated SV profiles for Triton X-100 micelles and such a complex. The boundaries for both the complex and the Triton X-100 micelles are sharp. Obviously this is not the case in the experiments (Figure 4a,c,g) where the boundaries are drawn out, as expected from the $c(s)$ analysis (Figure 4e). Note also that we observe, as in ref *10*, an invariance of the mean s value with dilution, which can be explained by a slow kinetics of equilibrium, if any.

In Figure 4f, the boundary profiles of the sample in D_2O buffer are presented. While the Triton X-100 micelles float, the protein complexes sediment slowly. Their mean sedimentation coefficient is $s = 0.9 \pm 0.2$ S. The combination of this value with the mean value of 5 S obtained in H_2O buffer provides an estimate of $\bar{v} = 0.89 \pm 0.18$ mL/g for the partial specific volume of the complex. It is compatible with a binding ratio of $B_d = 1.5$ g/g of Triton X-100 and $B_l = 0.25-1$ g/g of lipid (theoretical values of $\bar{v} = 0.86-0.89$ mL/g). The sedimentation boundaries of the complexes have a J/A_{278} ratio of 1.3. We calculate theoretical values of 1.1 or 1.3 for complexes with 1.5 g/g of Triton X-100 and 0.25 or 1 g/g of lipid, respectively. Thus J/A_{278} and experimental values of the partial specific volume of the complexes are compatible with $B_d = 1.5$ g/g, $B_l = 0.25$ g/g determined by Hackenberg and Klingenberg (*10*) but modeled better with a larger B_l ratio of 1 g/g of lipid. We consider these ranges of ratios to calculate, for globular compact assemblies ($f/f_0 = 1.25$), s values for monomer of 2.6 ± 0.1 S, for dimer of 4.1 ± 0.1 S, for trimer of 5.4 ± 0.1 S, and for tetramer of 6.9 ± 0.25 S. These correspond to the experimental range of s values for the main part of bAAC1 solubilized in Triton X-100. Minor contributions may correspond to octamers, with a calculated value of 10.4 ± 0.3 S. Chemical analyses on bAAC in a separate experiment, after sucrose gradient and before dialysis, provided a value of 0.4 g/g of bound phospholipid, compatible with the estimates from SV. The ratio of Triton X-100 over protein was ∼5 g/g, larger than our estimates from SV, probably because it takes into account free detergent micelles. Considering such a ratio would lead to calculation of $\bar{v} = 0.9$ mL/g, compatible with the estimate from SV, but $J/A_{278} = 0.8$, significantly lower than the experimental value. Furthermore, the calculated s values for globular monomer, dimer, trimer, and tetramer would be 3.3, 5.3, 6.9, and 8.4 S. Thus the conclusions about the association state of bAAC1 would not change. The fact that the smallest species is a monomer is also confirmed when the values of the sedimentation coefficients obtained in H_2O and D_2O buffers were analyzed jointly (Table 2).

bAAC in Triton X-100 after Quick Purification without Removal of Detergent Excess. To assess whether or not the purification protocol used by us and by Hackenberg and Klingenberg (*10*) (comprising long sucrose gradient and dialysis steps) could explain bAAC heterogeneity, we tested a rapid purification strategy. This alternative protocol allowed purification in hours instead of days. Bovine heart mitochondria were treated either with CATR or with bongkrekic acid (BA). bAAC was then solubilized with 3% Triton X-100 and purified on hydroxyapatite (HA) and size-exclusion (SEC) AcA columns in 0.02% Triton X-100. Buffer exchange to deuterated solvent was done with small desalting P6DG columns, and sedimentation velocity was performed at 20 °C.

Because of the strong absorbance of Triton X-100, only sedimentation velocity profiles obtained with interference optics can be used for analysis. bAAC−CATR and bAAC−BA behave similarly. The bAAC signal represents only ∼3% of the total signal, which is dominated by Triton X-100. bAAC is detected mainly at $s = 3.3-4.0$ S from the $c(s)$ analysis, and between 3 and 3.3 S from a noninteracting species analysis, with low amounts of larger ill-defined species also. Experiments in D_2O show the slow flotation and sedimentation of Triton X-100 micelles and bAAC complexes,

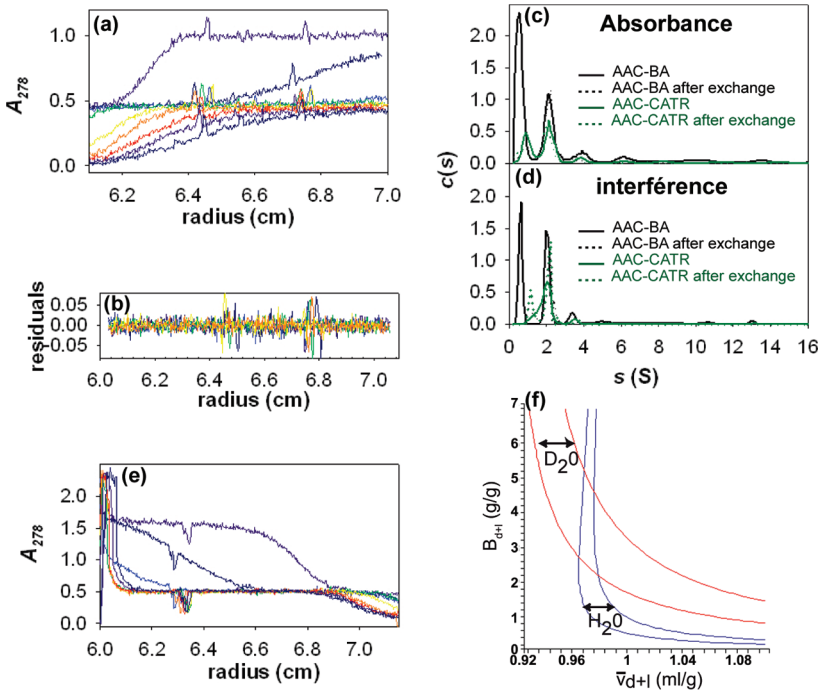

FIGURE 5: Sedimentation velocity experiments of bAAC1 in reduced Triton X-100. (a) Superimposition of selected experimental SV profiles for bAAC1−CATR sample in hydrogenated buffer, acquired at 278 nm after 11, 25, 38, 52, 108, 163, 229, 276, and 332 min at 42 000 rpm, at 20 °C, in 12 mm cells. (b) Residuals of the $c(s)$ analysis for the slow boundary in panel a (data during the first 40 min, corresponding to sedimentation of the large aggregates, are omitted). (c, d) Superimposition of the $c(s)$ analyses from data obtained at 278 nm and by use of interference, for bAAC1−CATR and bAAC1−BA, before and after solvent exchange on a P6DG column, all in hydrogenated buffer. (e) Superimposition of selected experimental profiles of bAAC1−CATR sample after solvent exchange on P6DG column to deuterated buffer. Experimental conditions are as in panel a, except there is a shift of 5 min in the times of data acquisition. (f) The implicit $B_{d+1} = f(\bar{v}_{d+1})$ function is drawn for f/f_0 ratio of 1.25 and considering a monomer for experimental s values for the main complex in H_2O (blue lines, corresponding to lower and higher values within the uncertainty range) and in D_2O (red lines). The existence of an intersection area between the curves in H_2O and those in D_2O for the monomer model demonstrates that this hypothesis is correct.

respectively (see Supporting Information Figure SI-3). Unfortunately, these data do not resolve whether bAAC is a dimer or a monomer (Table 2).

Solubilized bAAC in Reduced Triton X-100 Is Mainly Monomer after Quick Purification. Reduced Triton X-100 was then used with the same quick purification protocol, because its low absorbency allows the use of absorbency and interference optics in SV experiments. The elution profiles obtained upon the AcA column presented a shoulder, but the fractions for the whole peaks were pooled. For bAAC−CATR as for bAAC−BA, three samples were measured in SV: one directly from the AcA column and two after a further solvent-exchange column in either hydrogenated or deuterated solvents. The two samples in H_2O buffer before and after solvent exchange behave similarly, with only minor differences in the relative proportions of the different species.

We observe for typically half the total absorbance, for bAAC−CATR and bAAC−BA, very large aggregates that are centrifuged in 40 min at 42 000 rpm (Figure 5a). They have mean s values of ∼50 S in H_2O. Apart from the large aggregates, bAAC complexes are detected at 2 ± 0.1 S for the main monomer species (∼70%), 3.5 ± 0.5 S for the dimer (∼15%), and as small aggregates in the range 5−20 S (∼15%), as shown in Figure 5b−d. The analysis leading to determination of the association state is given below. Reduced Triton X-100 micelles sediment at 0.6−0.9 S and are hardly detected, as in the reference buffer by itself (not shown).

To interpret the SV experiments in terms of complex composition and association state, we analyze the $\bar{v}$ values inferred from complementary SV in D_2O solvent and the J/A_{278} ratios. In D_2O solvents, reduced Triton X-100 micelles float as expected (in the range −1 to −2 S), but surprisingly, so does bAAC (Figure 5e). Deconvolution between the species is difficult, except for the large aggregates, which float with a mean value of −40 S. We estimate $s \sim -0.1$ S (in the range 0 to −0.8 S) for bAAC smaller complexes. These values, combined with those in H_2O solvent, allows estimates of $\bar{v} = 0.95 \pm 0.1$ mL/g for the large aggregates and in the range 0.91−0.96 mL/g for the smaller complexes. The J/A_{278} ratio is estimated for bAAC small complexes with large errors (because of the complexity of the sample and the low values of s): in H_2O buffer, we estimate $J/A_{278} \sim 7$ for bAAC−CATR after solvent exchange and 15−18 for the other samples. The minimum value of 4 is found for the very large aggregates. The difference is probably not related to a difference in composition, since $\bar{v}$ is similar for the aggregates and for the main species, but to the low accuracy or maybe to scattering effects related to the large size of the particles.

The large values of $\bar{v}$ and of the J/A_{278} ratio suggest that bAAC complexes solubilized by reduced Triton X-100 contain a significantly increased amount of lipid when compared to the complexes in Triton X-100. Analysis of the s values obtained in H_2O and D_2O in terms of (B_{d+l}, $\bar{v}_{d+l}$) solutions, with bAAC considered as a monomer, are presented in Figure 5f. It gives $B_{d+l} = 4 \pm 1.5$ g/g and $\bar{v}_{d+l} =$

0.97 ± 0.01 mL/g when globular compact particles are considered with $f/f_0 = 1.25$ ($B_{d+l} = 5 \pm 1.5$ g/g and $\bar{v}_{d+l} = 0.96 \pm 0.01$ mL/g if $f/f_0 = 1.5$). These values are compatible with, for example, 1.5 and 2.5 g/g of reduced Triton X-100 and lipids, respectively. Analysis where a dimer is considered allows us to reject this hypothesis (Table 2).

DISCUSSION

To explore the controversial oligomeric state of bovine AAC, we performed analytical ultracentrifugation and neutron scattering experiments in various detergents. Our results clearly demonstrate that the protein is a monomer under a range of experimental conditions (i.e., bovine AAC solubilized in LAPAO and in reduced Triton X-100) and not a well-defined dimer as initially thought. In most of the conditions (i.e., Triton X-100 and reduced Triton X-100), oligomeric assemblies are also evidenced. Taken together with a critical review of some of the earlier experimental reports, these results might shed new light on the functional state of mitochondrial carriers, which could be in favor of supramolecular assemblies.

New Light on Old Data. The founding biophysical experiments that established the dimer hypothesis were performed by Hackenberg and Klingenberg (*10*) in 1980 and by Block et al. (*9*) in 1982 on bovine AAC. The first one identified a dimer of the bovine protein solubilized in Triton X-100 by ultracentrifugation. We repeated these experiments and found that under their experimental conditions the sample did not contain a single dimeric species but a mixture of monomers, dimers, trimers, and higher oligomers. In fact, the tremendously increased computational power of today's software compared to the 1980s made the analysis of our results more accurate and reliable, especially in difficult experimental conditions with a UV-absorbing detergent. Accurate analysis in terms of mixtures of several oligomeric species was also not possible at that time. Simulated profiles for the dimeric model are now available and they show a clear discrepancy with both Hackenberg and Klingenberg's and our experimental profiles: a sharp protein boundary is expected for a pure dimer, which is not present in the SV data (compare Figures 4 panels a, g, and h). Their data and ours are essentially the same, including the fact that dilution of the sample does not affect the proportion of the oligomeric states. However, the present analysis definitely establishes that the sample is not a dimer but a mixture of monomers, dimers, trimers, and higher oligomers. It should be argued that sample preparation was long and complex in these experiments and led to relatively low concentrations of Triton X-100 (they were minimized for the AUC experiments) of 2−4 times the cmc. These conditions should favor secondary aggregations (*28, 46, 50*). Since progress in SV analysis now allows us to decipher complex systems, we measured bAAC1 in a rapid protocol without minimization of Triton X-100 concentration. The protein signal is very low when compared to the detergent; our data suggest that the protein was much more homogeneous but the analysis could not determine whether the protein is a monomer or a dimer. We thus used the same protocol with reduced Triton X-100. In these conditions, the amount of bound lipid is larger and about half of the material sediments as very large aggregates. In the remaining, bAAC is mainly a monomer with ∼15% dimer and ∼15% other small multimers.

The neutron scattering work by Block et al. (*9*), who concluded that bAAC in the presence of LAPAO was a dimer, was also repeated, with similar starting material and sample purification protocol. We now have an increased knowledge of the sample complexity. Particularly, the unusually high detergent and lipid over protein ratio seriously impacts the calculated gyration radius and particle mass values. This problem arises because one cannot expect to match the scattering contribution of detergent and lipids when they are in 1000-fold (*31*) and 170-fold excess (this work) respectively. Actually, given the uncertainty on the matching point determination, the gyration radius value of 30 Å measured by Block et al. (*9*) and by us may be compatible with a monomer of AAC surrounded by detergent (data not shown), while the particle mass value is imprecise (1.5 times the theoretical value of the monomer). This is consistent with the AUC results, obtained with the same samples, which clearly show evidence of a monomer.

Therefore, we demonstrate here that the interpretations in terms of dimer of the published ultracentrifugation and neutron scattering works, for bAAC1 in Triton X-100 (*10*) and in LAPAO (*9*), respectively, were not correct. The samples were most probably also monomeric, with a significant fraction of higher molecular mass species for the Triton X-100-solubilized protein. The protocol used for preparation of the protein in the presence of LAPAO corresponds to the crystallization conditions of bovine AAC.

Stoichiometry of Inhibitor Binding. The very first piece of data in favor of a dimer came in the late 1970s from the unexpected finding that it is sufficient to add one CATR molecule per two AAC units to completely abolish the transport (*6, 7*). Although protein quantification by the Lowry method bears an important uncertainty, the measurements exclude a 1:1 ratio. The stoichiometry of BA binding is also often cited in favor of the dimer. However, it varies strongly with the extraction protocol of the protein from the mitochondrial membrane (*51*). Without added ADP, the inhibitor/protein ratio is the same for BA and CATR, but with ADP and a Brij extraction, the BA binding is 3 times the CATR binding. Such variation is explained by the amphipatic nature of this compound that could be easily trapped nonspecifically in detergent micelles. This makes the interpretation of BA binding unreliable for oligomeric state issues.

Since in the crystal structure each monomer bears a CATR molecule, the above-described observation remains puzzling. However, we may point out that the existence of a dimer is not the only way to explain the binding of one CATR to two proteins. Alternative scenarios are that half of the protein in the membrane may be not functional (immature or aged proteins, in relation to their natural turnover), and/or half may be spatially inaccessible; supramolecular arrangements could prevent a 1:1 binding ratio because of steric hindrance. In the case of the Ca^{2+}-ATPase from sarcoplasmic reticulum, whose functional unit is a monomer, it is not possible (without clear explanation) to reach 100% phosphorylation from ATP (see, for example, ref *52* and references therein). Also, for AAC, it was shown that CATR binding exhibits cooperativity enhanced by ATP (*53, 54*). Interestingly, in ref *53*, it is shown that sonication suppresses the cooperativity of CATR binding, which could suggest the existence of a somewhat fragile supramolecular complex containing AAC.

Yeast AAC Is a Monomer. In *n*-dodecyl β-D-maltopyranoside (DDM) or other detergents, from size-exclusion chromatography (*21*), sedimentation equilibrium (*21*), and differential tagging (*22*) experiments, yeast AAC is a monomer. In DDM, after detergent binding measurement and by SE and SV, we also found that yeast AAC3 is a monomer (data not shown), confirming the data of Bamber et al. (*21*).

Bamber et al. (*23*) showed the monomer can achieve transport in the mitochondrial membrane. However, the measured transport rate (20 nmol of ADP mg^{-1} min^{-1}) is only a tiny fraction of the expected transport rate in vivo [3 × 10^4 (*55*) to 3 × 10^5 (*56*) nmol of ADP mg^{-1} min^{-1}]. Some explanation can be provided by this fact: the external concentration of substrate used in these experiments is at least 1000-fold below estimated concentrations present in mitochondria. If Michaelis−Menten kinetics apply, the rate will thus consequently be a fraction of the V_{max}. In addition, the conditions are unfavorable: for instance, temperature, maintenance of gradients, etc. Thus, the lower rates are not necessarily indicative of a large fraction of inactive protein but could be simply a consequence of kinetics at low substrate concentrations and temperature. In addition, the study by Bamber et al. (*23*) used fused mitochondrial membranes, which showed marginally higher transport rates than membranes with reconstituted carriers. Since in this case there is no reason to suspect that there is a large inactive fraction, as the carriers never left the membranes, one can suggest that the lower rates of transport are not due to reconstitution defects. It would be very interesting to be able to reconstitute carrier with transport activities similar to the one measured in mitochondria.

Chimeric dimers were built and found to be functional (*16*); wild-type and chimeric dimer proteins have similar activities (for a similar total amount). But conclusions about oligomeric state based on the comparison of activities are not definitive: not all the carriers probably participate in transport at a given time, and monomers could work side by side. However, cooperativity within heterodimers of phosphate and ADP/ATP carriers (*57*) is more difficult to interpret if solely a monomeric functional AAC is considered. Another apparent contradiction lies in the divergent conclusions from native electrophoresis, which suggest oligomeric structure (*13, 14*), while differential tagging, in similar experimental conditions in DDM, demonstrates only the monomer (*22*).

Slight Differences in the Experimental Conditions Sometimes Reveal Multimeric Species. Although most of our experiments are indicative of a monomeric AAC, some of them point to some preferential interaction of AAC with itself. This interaction is unambiguously demonstrated in sedimentation velocity experiments with bAAC1 in Triton X-100, following the purification protocol of Hackenberg and Klingenberg (*10*), or with bAAC1 in reduced Triton X-100, following the quick purification protocol as seen in Figures 4 and 5. However, our results also show that the dimer does not prevail over the other association states. Cross-linking experiments in our hands (for yeast AAC) are not in favor of a dimer either (*58*).

Dense Packing versus Dimers. Because the debate was centered on the monomer−dimer (potentially tetramer) question, macromolecular crowding and dense packing effects were hardly ever discussed. Given the abundance of AAC in bovine mitochondria, one can consider the possibility of a supermolecular organization in dense patches rather than well-defined oligomers. This patches might be revealed by the very large aggregates (average 50 S) observed in reduced Triton X-100 (Figure 5a,e). Bamber et al. (*21*) have observed, in the absence of inhibitors and after gel filtration and reconstitution into liposomes, small nonfunctional aggregates. Although we have not performed functional tests in the framework of the present study, we could hypothesize that the large multimers obtained in the presence of BA or CATR are somehow reminiscent of assemblies within the lipid membrane. If patches exist, they may play a role in the stability and efficiency of the transport, yielding a higher probability for nucleotides to cross the membrane.

The 3D high-resolution structure of bovine AAC in complex with CATR is a bundle of six tilted helices with a wide cavity open to the intermembrane space. Though a single structure does not explain the transport mechanism, it looks compatible with a monomer. Because the cavity is wide, and as possible conformation changes are considered, a monomer could accommodate both substrates. However, within the helical bundle, each individual helix faces both lipids in the membrane and solvent in the cavity, thus revealing a rather fragile structure. A dense packing involving cardiolipins could stabilize the protein laterally.

The lateral surface of the protein, on the region corresponding to the inner leaflet of the membrane, is occupied by three tightly bound cardiolipin molecules. Therefore, from the CATR-bound structure, all putative interfaces must be mediated partly by lipid−lipid or lipid−protein interactions. This is the case in interactions between monomers in the crystals (*20*). While such interactions are satisfactory in a dense packing scenario, they might be insufficient for a functional mandatory coupling. Moreover, analysis of the lateral surface residues regarding conservation among the AACs, or complementary patches (such as a negatively charged patch matching a positive one on another monomer), does not highlight any specific area (*59*).

Inner Membrane Topology. The topology of the inner membrane is both complex and dynamic, as imaged by EM tomography (*60*). Rows of ATP synthase dimers (*61*) are believed to participate in the shape of cristae (*62*). AAC could also influence the inner membrane shape: tomographs of mitochondria from a patient suffering Senger syndrome, a disease characterized by depletion of isoform 1 of AAC, display vesicular cristae very different from normal topology (*63*). Moreover, Scherer and Klingenberg (*64*) reported long ago contraction and expansion of the matrix monitored by absorbency at 546 nm upon addition of BA and ATR, respectively. It is tempting, though very speculative, to link topology modification and packing of the AACs.

CONCLUSIONS

Structural and functional properties of native membranes result from molecular determinants and their organization from the atomic to the mesoscopic scale. Therefore, supramolecular assemblies fill the gap between single molecules and microscopic features of the organelle. Our work is in better agreement with loose assemblies of AAC than with well-defined dimers. The existence of such assemblies and their impact at the mesoscopic scale are still difficult to

evidence. The functioning of AAC within the mitochondria remains a debated conjecture.

ACKNOWLEDGMENT

We dedicate this paper to the memory of Professor Pierre Vignais, who passed away in September 2006. He made major contributions to the mitochondrial field and in the topics of ADP/ATP carriers and stimulated this work. We thank J. Zaccaï (Institut Laue Langevin and Institut de Biologie Structurale, Grenoble, France) for his help for the neutron scattering experiments.

SUPPORTING INFORMATION AVAILABLE

Figure SI-1, graphical determination of the match point for LAPAO/lipid samples in SANS experiments of bAAC; Figure SI-2, Guinier plot from SANS of bAAC/LAPAO/lipid sample at 15% D_2O; and Figure SI-3, sedimentation velocity of bAAC−CATR and bAAC−BA after quick purification in Triton X-100. This material is available free of charge via the Internet at http://pubs.acs.org.

REFERENCES

1. Walker, J. E., and Runswick, M. J. (1993) The mitochondrial transport protein superfamily. *J. Bioenerg. Biomembr. 25*, 435–446.
2. Palmieri, F. (2004) The mitochondrial transporter family (SLC25): physiological and pathological implications. *Pflugers Arch. 447*, 689–709.
3. Nury, H., Dahout-Gonzalez, C., Trézéguet, V., Lauquin, G. J., Brandolin, G., and Pebay-Peyroula, E. (2006) Relations between structure and function of the mitochondrial ADP/ATP carrier. *Annu. Rev. Biochem. 75*, 713–741.
4. Klingenberg, M. (2008) The ADP and ATP transport in mitochondria and its carrier. *Biochim. Biophys. Acta: Biomembr. 1778*, 1978–2021.
5. Pebay-Peyroula, E., Dahout-Gonzalez, C., Kahn, R., Trézéguet, V., Lauquin, G. J., and Brandolin, G. (2003) Structure of mitochondrial ADP/ATP carrier in complex with carboxyatractyloside. *Nature 426*, 39–44.
6. Riccio, P., Aquila, H., and Klingenberg, M. (1975) Purification of the carboxy-atractylate binding protein from mitochondria. *FEBS Lett. 56*, 133–138.
7. Klingenberg, M., Riccio, P., and Aquila, H. (1978) Isolation of the ADP, ATP carrier as the carboxyatractylate • protein complex from mitochondria. *Biochim. Biophys. Acta 503*, 193–210.
8. Brandolin, G., Doussiere, J., Gulik, A., Gulik-Krzywicki, T., Lauquin, G. J., and Vignais, P. V. (1980) Kinetic, binding and ultrastructural properties of the beef heart adenine nucleotide carrier protein after incorporation into phospholipid vesicles. *Biochim. Biophys. Acta 592*, 592–614.
9. Block, M. R., Zaccaï, G., Lauquin, G. J., and Vignais, P. V. (1982) Small angle neutron scattering of the mitochondrial ADP/ATP carrier protein in detergent. *Biochem. Biophys. Res. Commun. 109*, 471–477.
10. Hackenberg, H., and Klingenberg, M. (1980) Molecular weight and hydrodynamic parameters of the adenosine 5′-diphosphate−adenosine 5′-triphosphate carrier in Triton X-100. *Biochemistry 19*, 548–555.
11. Majima, E., Ikawa, K., Takeda, M., Hashimoto, M., Shinohara, Y., and Terada, H. (1995) Translocation of loops regulates transport activity of mitochondrial ADP/ATP carrier deduced from formation of a specific intermolecular disulfide bridge catalyzed by copper-o-phenanthroline. *J. Biol. Chem. 270*, 29548–29554.
12. Hashimoto, M., Majima, E., Goto, S., Shinohara, Y., and Terada, H. (1999) Fluctuation of the first loop facing the matrix of the mitochondrial ADP/ATP carrier deduced from intermolecular cross-linking of Cys56 residues by bifunctional dimaleimides. *Biochemistry 38*, 1050–1056.
13. Dyall, S. D., Agius, S. C., De Marcos Lousa, C., Trezeguet, V., and Tokatlidis, K. (2003) The dynamic dimerization of the yeast ADP/ATP carrier in the inner mitochondrial membrane is affected by conserved cysteine residues. *J. Biol. Chem. 278*, 26757–26764.
14. Faustin, B., Rossignol, R., Rocher, C., Benard, G., Malgat, M., and Letellier, T. (2004) Mobilization of adenine nucleotide translocators as molecular bases of the biochemical threshold effect observed in mitochondrial diseases. *J. Biol. Chem. 279*, 20411–20421.
15. Hatanaka, T., Hashimoto, M., Majima, E., Shinohara, Y., and Terada, H. (1999) Functional expression of the tandem-repeated homodimer of the mitochondrial ADP/ATP carrier in *Saccharomyces cerevisiae*. *Biochem. Biophys. Res. Commun. 262*, 726–730.
16. Trézéguet, V., Le Saux, A., David, C., Gourdet, C., Fiore, C., Dianoux, A., Brandolin, G., and Lauquin, G. J. (2000) A covalent tandem dimer of the mitochondrial ADP/ATP carrier is functional in vivo. *Biochim. Biophys. Acta 1457*, 81–93.
17. Huang, S. G., Odoy, S., and Klingenberg, M. (2001) Chimers of two fused ADP/ATP carrier monomers indicate a single channel for ADP/ATP transport. *Arch. Biochem. Biophys. 394*, 67–75.
18. Pebay-Peyroula, E., and Brandolin, G. (2004) Nucleotide exchange in mitochondria: insight at a molecular level. *Curr. Opin. Struct. Biol. 14*, 420–425.
19. Kunji, E. R., and Harding, M. (2003) Projection structure of the atractyloside-inhibited mitochondrial ADP/ATP carrier of *Saccharomyces cerevisiae*. *J. Biol. Chem. 278*, 36985–36988.
20. Nury, H., Dahout-Gonzalez, C., Trézéguet, V., Lauquin, G., Brandolin, G., and Pebay-Peyroula, E. (2005) Structural basis for lipid-mediated interactions between mitochondrial ADP/ATP carrier monomers. *FEBS Lett. 579*, 6031–6036.
21. Bamber, L., Harding, M., Butler, P. J., and Kunji, E. R. (2006) Yeast mitochondrial ADP/ATP carriers are monomeric in detergents. *Proc. Natl. Acad. Sci. U.S.A. 103*, 16224–16229.
22. Bamber, L., Slotboom, D. J., and Kunji, E. R. (2007) Yeast mitochondrial ADP/ATP carriers are monomeric in detergents as demonstrated by differential affinity purification. *J. Mol. Biol. 371*, 388–395.
23. Bamber, L., Harding, M., Monne, M., Slotboom, D. J., and Kunji, E. R. (2007) The yeast mitochondrial ADP/ATP carrier functions as a monomer in mitochondrial membranes. *Proc. Natl. Acad. Sci. U.S.A. 104*, 10830–10834.
24. Musatov, A., and Robinson, N. C. (2002) Cholate-induced dimerization of detergent- or phospholipid-solubilized bovine cytochrome *c* oxidase. *Biochemistry 41*, 4371–4376.
25. Veenhoff, L. M., Heuberger, E. H., and Poolman, B. (2002) Quaternary structure and function of transport proteins. *Trends Biochem. Sci. 27*, 242–249.
26. Heuberger, E. H., Veenhoff, L. M., Duurkens, R. H., Friesen, R. H., and Poolman, B. (2002) Oligomeric state of membrane transport proteins analyzed with blue native electrophoresis and analytical ultracentrifugation. *J. Mol. Biol. 317*, 591–600.
27. Chabre, M., and le Maire, M. (2005) Monomeric G-protein-coupled receptor as a functional unit. *Biochemistry 44*, 9395–9403.
28. le Maire, M., Møller, J. V., Menguy, T., Velours, J., and Champeil, P. (2007) Protein−protein contacts in solubilized membrane proteins, as detected by cross-linking. *Anal. Biochem. 362*, 168–171.
29. Lauquin, G. J., and Vignais, P. V. (1976) Interaction of [^{3}H]bongkrekic acid with the mitochondrial adenine nucleotide translocator. *Biochemistry 15*, 2316–2322.
30. Bartlett, G. R. (1959) Phosphorus assay in column chromatography. *J. Biol. Chem. 234*, 466–468.
31. Dahout-Gonzalez, C., Brandolin, G., and Pebay-Peyroula, E. (2003) Crystallization of the bovine ADP/ATP carrier is critically dependent upon the detergent-to-protein ratio. *Acta Crystallogr. D: Biol. Crystallogr. 59*, 2353–2355.
32. Krämer, R., and Klingenberg, M. (1977) Reconstitution of adenine nucleotide transport with purified ADP, ATP-carrier protein. *FEBS Lett. 82*, 363–367.
33. Jacrot, B., and Zaccaï, G. (1981) Determination of molecular weight by neutron scattering. *Biopolymers 20*, 2423–2426.
34. Ebel, C. (2007) Solvent mediated protein−protein interactions, in *Protein Interactions: Biophysical Approaches for the Study of Complex Reversible Systems* (Schuck, P., Ed.) pp 255−287, Springer, Berlin.
35. le Maire, M., Møller, J. V., and Tardieu, A. (1981) Shape and thermodynamic parameters of a Ca^{2+}-dependent ATPase. A solution X-ray scattering and sedimentation equilibrium study. *J. Mol. Biol. 150*, 273–296.

36. Gohon, Y., Pavlov, G., Timmins, P., Tribet, C., Popot, J.-L., and Ebel, C. (2004) Partial specific volume and solvent interactions of amphipol A8−35. *Anal. Biochem. 334*, 318–334.
37. Salvay, A. G., Santamaria, M., le Maire, M., and Ebel, C. Analytical Ultracentrifugation Sedimentation Velocity for the Characterization of Detergent−Solubilized Membrane Proteins Ca^{++}-ATPase and ExbB, *J. Biol. Phys.* (in press).
38. Schuck, P. (2000) Size-distribution analysis of macromolecules by sedimentation velocity ultracentrifugation and lamm equation modeling. *Biophys. J. 78*, 1606–1619.
39. Manon, F., and Ebel, C. Analytical ultracentrifugation, a useful tool to probe intrinsically disordered proteins, in *Instrumental Analysis of Intrinsically Disordered Proteins: Assessing Structure and Conformation* (Uversky, V., and Longhi, S., Eds.) John Wiley and Sons, New York (in press).
40. Ebel, C. (2007) Analytical ultracentrifugation. State of the art and perspectives, in *Protein Structures: Methods in Protein Structure and Stability Analysis* (Uversky, V., and Permyakov, E. A., Eds.), pp 229−260, Nova Science Publishers, New York.
41. Ebel, C., Møller, J. V., and le Maire, M. (2007) Analytical ultracentrifugation: membrane protein assemblies in the presence of detergent, in *Biophysical analysis of membrane proteins: Investigating structure and function* (Pebay-Peyroula, E., Ed.), pp 91−120, Wiley, New York.
42. le Maire, M., and Møller, J. V. (1981) Size and shape of membrane proteins: some improved procedures. *Biochimie 63*, 863–866.
43. Huang, C., and Charlton, J. P. (1971) Studies on phosphatidylcholine vesicles. Determination of partial specific volumes by sedimentation velocity method. *J. Biol. Chem. 246*, 2555–2560.
44. Salvay, A. G., and Ebel, C. (2006) Analytical ultracentrifuge for the characterization of detergent in solution. *Prog. Colloid Polym. Sci. 131*, 74–82.
45. Hayashi, Y., Matsui, H., and Takagi, T. (1989) Membrane proteins molecular weight determined by low angle laser light-scattering photometry coupled with high-performance gel chromatography. *Methods Enzymol. 172*, 514–528.
46. le Maire, M., Champeil, P., and Møller, J. V. (2000) Interaction of membrane proteins and lipids with solubilizing detergents. *Biochim. Biophys. Acta 1508*, 86–111.
47. Hunt, J. F., McCrea, P. D., Zaccai, G., and Engelman, D. M. (1997) Assessment of the aggregation state of integral membrane proteins in reconstituted phospholipid vesicles using small angle neutron scattering. *J. Mol. Biol. 273*, 1004–1019.
48. Lipfert, J., and Doniach, S. (2007) Small-angle X-ray scattering from RNA, proteins, and protein complexes. *Annu. Rev. Biophys. Biomol. Struct. 36*, 307–327.
49. Reynolds, J. A., and Tanford, C. (1976) Determination of molecular weight of the protein moiety in protein−detergent complexes without direct knowledge of detergent binding. *Proc. Natl. Acad. Sci. U.S.A. 73*, 4467–4470.
50. Møller, J. V., le Maire, M., and Andersen, J. P. (1988) Use of detergents to solubilize the Ca^{2+}-pump protein as monomers and defined oligomers. *Methods Enzymol. 157*, 261–270.
51. Aquila, H., Eiermann, W., Babel, W., and Klingenberg, M. (1978) Isolation of the ADP/ATP translocator from beef heart mitochondria as the bongkrekate−protein complex. *Eur. J. Biochem. 85*, 549–560.
52. Menguy, T., Corre, F., Bouneau, L., Deschamps, S., Møller, J. V., Champeil, P., le Maire, M., and Falson, P. (1998) The cytoplasmic loop located between transmembrane segments 6 and 7 controls activation by Ca^{2+} of sarcoplasmic reticulum Ca^{2+}-ATPase. *J. Biol. Chem. 273*, 20134–20143.
53. Vignais, P. V., Vignais, P. M., and Defaye, G. (1973) Adenosine diphosphate translocation in mitochondria. Nature of the receptor site for carboxyatractyloside (gummiferin). *Biochemistry 12*, 1508–1519.
54. Vignais, P. V., Vignais, P. M., and Defaye, G. (1971) Gummiferin, an inhibitor of the adenine-nucleotide translocation. Study of its binding properties to mitochondria. *FEBS Lett. 17*, 281–288.
55. Vignais, P. V. (1976) Molecular and physiological aspects of adenine nucleotide transport in mitochondria. *Biochim. Biophys. Acta 456*, 1–38.
56. Gropp, T., Brustovetsky, N., Klingenberg, M., Müller, V., Fendler, K., and Bamberg, E. (1999) Kinetics of electrogenic transport by the ADP/ATP carrier. *Biophys. J. 77*, 714–726.
57. Postis, V., De Marcos Lousa, C., Arnou, B., Lauquin, G. J., and Trézéguet, V. (2005) Subunits of the yeast mitochondrial ADP/ATP carrier: cooperation within the dimer. *Biochemistry 44*, 14732–14740.
58. Arnou, B. (2006) Le transporteur mitochondrial de nucléotides adényliques de S. cerevisiae: état oligomérique et cristallogenèse tridimensionnelle, Ph.D. Thesis, Institut de Biochimie et Génétique Cellulaires, Université Victor Segalen Bordeaux 2, Bordeaux, France.
59. Nury, H. (2007) Etudes structurales du transporteur mitochondrial d'ADP et d'ATP, PhD Thesis, Institut de Biologie Structurale, Université Joseph Fourier, Grenoble, France.
60. Mannella, C. A. (2006) The relevance of mitochondrial membrane topology to mitochondrial function. *Biochim. Biophys. Acta 1762*, 140–147.
61. Buzhynskyy, N., Sens, P., Prima, V., Sturgis, J. N., and Scheuring, S. (2007) Rows of ATP synthase dimers in native mitochondrial inner membranes. *Biophys. J. 93*, 2870–2876.
62. Strauss, M., Hofhaus, G., Schroder, R. R., and Kuhlbrandt, W. (2008) Dimer ribbons of ATP synthase shape the inner mitochondrial membrane. *EMBO J. 27*, 1154–1160.
63. Mannella, C. A. (2006) The relevance of mitochondrial membrane topology to mitochondrial function. *Biochim. Biophys. Acta 1762*, 140–147.
64. Scherer, B., and Klingenberg, M. (1974) Demonstration of the relationship between the adenine nucleotide carrier and the structural changes of mitochondria as induced by adenosine 5′-diphosphate. *Biochemistry 13*, 161–170.

BI801053M